# Polyelectrolyte Layer-by-Layer Assembly To Control the Distance between Fluorophores and Plasmonic Nanostructures

Krishanu Ray, Ramachandram Badugu, and Joseph R. Lakowicz*

*Center for Fluorescence Spectroscopy, Department of Biochemistry and Molecular Biology, University of Maryland School of Medicine, 725 West Lombard Street, Baltimore, Maryland 21201*

*Received June 5, 2007. Revised Manuscript Received August 31, 2007*

In the past several years we have demonstrated the metal-enhanced fluorescence (MEF) and the significant changes in the photophysical properties of fluorophores in the presence of metallic nanostructures and nanoparticles. MEF is largely dependent on several factors, such as chemical nature, size, shape of the nanostructure, and its distance from the interrogating fluorophore. Herein, we elucidate the potential of layer-by-layer (LbL) assembly to understand the distance dependence nature of MEF from sulforhodamine B (SRB) assembled on the plasmonic nanostructured surfaces [in the form of Silver Islands films (SIFs)]. The varied proximity of fluorophores from the SIF surfaces was controlled by constructing different numbers of alternate layers of poly(styrene sulfonate) (PSS) and poly(allylamine hydrochloride) (PAH). An anionic laser dye SRB could be electrostatically attached to the positively charged PAH layer. Orientation of the SRB probe molecule adsorbed in PSS/PAH-layered assembly was determined by polarized absorption spectroscopy. The observed tilt angle of the probe transition dipole moment with respect to the surface normal was 40°. Our results show that MEF is indeed distance-dependent. Accordingly, we observed a maximum of a ∼6-fold increase in the fluorescence intensity from a monolayer of the SRB at a distance of ∼9 nm from the metal-nanostructured surface, with the enhancement decreasing down to ∼1.5-fold at about a 30 nm separation distance. Consistently, the minimum lifetimes were about 4-fold shorter than those on glass slides without silver, with the lifetimes being about nearly the same for 15 layers of the PSS/PAH assembly. The intensity–time decays were analyzed with a lifetime distribution model to underpin the distance effect on the metal–fluorophore interaction in the nanometric range. The present study provides improved understanding of the interaction between plasmonic nanostructures and fluorophores and, more importantly, their distance dependence nature, where we used a robust, easy, and inexpensive alternate electrostatic LbL assembly as a bottom-up nanofabrication technique to control the probe distance from the surface.

## 1. Introduction

Plasmonic metal nanostructures and nanoparticles have received increased attention because of the tunability of their optical properties with the particle size, shape, and assembly process.[1–7] Silver nanostructues have strong optical absorption in the visible spectral region caused by excitation of collective oscillations of free electrons. The resonance frequency as well as the plasmon absorption band depends on the nanoparticle size and interactions between those. Metallic nanostructures enhance the local optical fields via localized plasmon resonances and thus improve the light absorption and emission process. These enhanced local field effects are one of the major reasons for observation of increased emission, which is known as metal-enhanced fluorescence (MEF)[8–14] of fluorophores near roughened or particulate metal surfaces.

MEF arises from the electromagnetic interactions that occur between fluorescent probes and metal nanoparticles that have appropriate enhancing optical properties. Under suitable conditions, the close proximity of fluorophores to metal particles has a dramatic effect on fluorescence quantum yields and lifetimes. Near-field interactions of the fluorophores with the metal can cause more rapid emission of the fluorophore.[1] We have shown that the metal nanoparticles could change the radiative decay rates of fluorophores.[9–12] These changes occur because of modifications of the photonic mode density near the particle. Using metal nanoparticles, we could engineer changes in the emission based on the fluorophore–metal particle geometries. This use of fluoro-

* E-mail: Lakowicz@cfs.umbi.umd.edu.

(1) Lakowicz, J. R. *Plasmonics* **2006**, *1*, 5.
(2) Lee, K.; El-Sayed, M. A. J. *Phys. Chem. B* **2005**, *109*, 20331.
(3) El-Sayed, M. A. *Acc. Chem. Res.* **2001**, *34*, 257.
(4) Wang, H.; Brandl, W.; Nordlander, P.; Halas, N. J. *Acc. Chem. Res.* **2007**, *40*, 53.
(5) Kreibig, U.; Vollmer, M. *Optical Properties of Metal Clusters*; Springer-Verlag:Berlin, 1995.
(6) Chen, J.; Wiley, B. J.; Xia, Y. *Langmuir* **2007**, *23*, 4120.
(7) Barnes, W. L. J. *Mod. Opt.* **1998**, *45*, 661.
(8) Geddes, C. D.; Lakowicz, J. R. J. *Fluorescence* **2002**, *12*, 121.
(9) Lakowicz, J. R. *Anal. Biochem.* **2001**, *298*, 1.
(10) Lakowicz, J. R. *Anal. Biochem.* **2005**, *337*, 171.
(11) Lakowicz, J. R.; Shen, Y.; D'Auria, S.; Malicka, J.; Fang, J.; Grcyzynski, Z.; Gryczynski, I. *Anal. Biochem.* **2002**, *301*, 261.
(12) Ray, K.; Badugu, R.; Lakowicz, J. R. *J. Am. Chem. Soc.* **2006**, *128*, 8998.
(13) Ray, K.; Badugu, R.; Lakowicz, J. R. *J. Phys. Chem. B* **2006**, *110*, 13499.
(14) Malicka, J.; Gryczynski, I.; Gryczynski, Z.; Lakowicz, J. R. *Anal. Biochem.* **2003**, *315*, 57.

10.1021/cm071510w CCC: $37.00 
Published on Web 11/03/2007

phore–metal interactions, also known as plasmon-controlled fluorescence, represents a paradigm shift in fluorescence detection using metallic nanostructures.[1] MEF is of great interest because of the widespread use of molecular fluorescence-based measurements and devices in chemistry, molecular biology, materials science, photonics, and medicine. Because of these applications, it is important to understand these interactions in terms of the effects of chemical nature, size, shape of the nanostructure, and its distance from the interrogating fluorophore.[15–19] A detail understanding of the MEF and its distance dependence nature is vital for its potential application in biomedical sensing.[20–22]

Layer-by-layer (LbL) assembly[23–36] is based on the sequential adsorption of polycations and polyanions from dilute aqueous solution onto a solid substrate as a consequence of the electrostatic interaction and complex formation between oppositely charged polyelectrolytes. Starting from a functionalized solid substrate, it is possible to adsorb a variety of charged species ranging from polyelectrolytes, nanoparticles, and ionic dyes to many biological agents such as viruses, proteins, and DNA. Over the past several years, the LbL technique has evolved into a versatile and powerful method to grow thin polymeric films on a variety of solid substrates. Importantly, LbL can be carried out at room temperature and it requires neither sophisticated instruments nor subsequent annealing of the deposited film, so that a wide variety of the substrates can be used. The spontaneous sequential adsorption of dissolved anionic and cationic polyelectrolytes leads to the formation of ordered multilayer assemblies on a solid substrate. The complete reversal of surface charge after each immersion is the crucial factor for a regular stepwise growth of the multilayer films. The ultrathin films formed by LbL assembly have been shown to be uniform and of precisely controllable thickness. The LbL adsorption technique is an easy and inexpensive process for multilayer formation and allows different types of materials to be incorporated into the film structures. Furthermore, with LbL assembly the distance between the spherical metal colloid and the fluorophore, as well as between planar metallic nanostructures and the fluorophore, could be controlled. The LbL method already shows fabrication of nanostructures with the positioning of target materials in desired geometries. The LbL assembly has been recently shown to be effective as a versatile bottom-up nanofabrication technique.

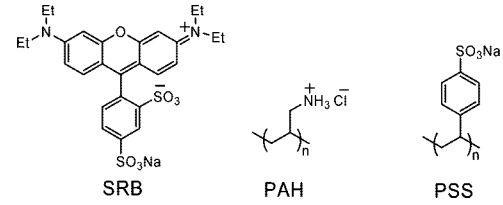


**Figure 1.** Molecular structures of SRB, PAH, and PSS.

In the present work, we take advantage of this simple well-established LbL technique to fabricate the samples with varied probe distances from the plasmonic nanostructured surface to reveal the distance effect on the MEF. In this LbL assembling process, multilayered structures of poly(styrene sulfonate) (PSS) and poly(allylamine hydrochloride) (PAH) are fabricated in a well-defined and controllable manner. Subsequently, anionic sulforhodamine B (SRB) is incorporated into the topmost positively charged PAH layer. The distance between SRB and the metal surface is modulated by using different numbers of PSS/PAH layers. Lavalle et al.[25] reported the growth of the PSS/PAH multilayers by means of in situ atomic force microscopy and by optical waveguide light-mode spectroscopy. These studies showed that PSS/PAH films followed a linear growth with the number of deposited layer pairs. The analysis of the structure of the PSS/PAH films reveals a smooth featureless surface covered by small globules. A detailed investigation using steady-state and time-resolved fluorescence spectroscopy has been carried out to unravel the distance effect on the MEF. By studying the distance dependence of molecular fluorescence enhancement by plasmonic nanostructures, we can gain a comprehensive understanding of metal–nanostructure/nanoparticle–fluorophore interactions at the nanoscale level. Increased understanding of this interaction will ultimately lead to design strategies for optimizing fluorescence enhancement with adjacent metallic nanostructures, a highly useful goal with direct relevance in many molecule-based measurement or device applications.

## 2. Experimental Details

Sodium salt of poly(styrene sulfonate) (PSS; MW 70000), poly(allylamine hydrochloride) (PAH; MW 50000–65000), sulforhodamine B (SRB; Figure 1), and cysteamine were obtained from Sigma-Aldrich-Fluka. Polyelectrolytes and other chemicals were used without further purification. Deionized water, purified using a Millipore Milli-Q gradient system with a resistivity of 18.2 MΩ·cm, was used for LbL assembly. Silver nitrate, ammonium hydroxide, sodium hydroxide, and D-glucose were obtained from

(15) Tarcha, P. J.; DeSaja-Gonzalez, J.; Rodriguez-LIorente, S.; Aroca, R. *Appl. Spectrosc.* **1999**, *53*, 43–48.
(16) Antunes, P. A.; Constantino, C. J. L.; Aroca, R. F.; Duff, J. *Langmuir* **2001**, *17*, 2958.
(17) Sokolov, K.; Chumanov, G.; Cotton, T. M. *Anal. Chem.* **1998**, *70*, 3898.
(18) Ray, K.; Badugu, R.; Lakowicz, J. R. *Langmuir* **2006**, *22*, 8374.
(19) Ray, K.; Badugu, R.; Lakowicz, J. R. *J. Phys. Chem. C* **2007**, *111*, 7091.
(20) Pompa, P. P.; Martiradonna, L.; Della Torre, A.; Della Sala, F.; Manna, L.; De Vittorio, M.; Calabi, F.; Cingolani, R.; Rinaldi, R. *Nat. Nanotechnol.* **2006**, *1*, 126.
(21) Aslan, K.; Wu, M.; Lakowicz, J. R.; Geddes, C. D. *J. Am. Chem. Soc.* **2007**, *129*, 1524.
(22) Aslan, K.; Huang, J.; Wilson, G. M.; Geddes, C. D. *J. Am. Chem. Soc.* **2006**, *128*, 4206.
(23) Decher, G. *Science* **1997**, *277*, 1232.
(24) Decher, G.; Hong, J. D.; Schmitt, J. *Thin Solid Films* **1992**, *210*, 831.
(25) Lavalle, P.; Gergely, C.; Cuisinier, F. J. G.; Decher, G.; Schaaf, P.; Voegel, J. C.; Picart, C. *Macromolecules* **2002**, *35*, 4458.
(26) Lvov, Y.; Decher, G.; Sukhorukov, G. *Macromolecules* **1993**, *26*, 5396.
(27) Lvov, Y.; Ariga, K.; Ichinose, I.; Kunitake, T. *J. Am. Chem. Soc.* **1995**, *117*, 6117.
(28) Caruso, F.; Caruso, R. A.; Moehwald, H. *Science* **1998**, *282*, 1111.
(29) Ariga, K.; Hill, J. P.; Ji, Q. *Phys. Chem. Chem. Phys.* **2007**, *9*, 2319.
(30) Tang, Z.; Wang, Y.; Podsidlo, P.; Kotov, N. A. *Adv. Mater.* **2006**, *18*, 3203.
(31) Love, J. C.; Estroff, L. A.; Kriebel, J. K.; Nuzzo, R. G.; Whitesides, G. M. *Chem. Rev.* **2005**, *105*, 1103.
(32) Fendler, J. H. *Chem. Mater.* **1996**, *8*, 1616.
(33) Hammond, P. T. *Adv. Mater.* **2004**, *16*, 1271.
(34) Whitesides, G. M.; Grzybowski, B. *Science* **2002**, *295*, 2418.
(35) Michinobu, T.; Nakanishi, T.; Hill, J. P.; Funahashi, M.; Ariga, K. *J. Am. Chem. Soc.* **2006**, *128*, 10384.
(36) Ruben, M.; Lehn, J. M.; Muller, P. *Chem. Soc. Rev.* **2006**, *35*, 1056.

Sigma-Aldrich and used as received. Premium-quality (aminopropyl)triethoxysilane (APS) coated glass slides were obtained from Sigma. Silver Island films (SIFs) were grown on the silanated glass slides using the method reported previously by us.[13] This procedure consists of reducing silver nitrate with D-glucose under controlled conditions and results in a partial coating of the slide with SIF. Briefly, about 1.5 mL of a freshly prepared 5% NaOH solution was added to a stirring aqueous silver nitrate solution (0.375 g in 45 mL of water) in a glass beaker. Subsequently, the resulting dark-brown precipitate was redissolved by slowly adding 1 mL of $NH_4OH$. The solution was cooled to 5 °C in an ice bath and a fresh solution of D-glucose (0.540 g in 11 mL of water) was added, followed by four pairs of APS-coated glass slides placed into this solution. The mixture was stirred for 2 min in an ice bath and then allowed to warm to 30 °C for the next 5 min. As the color of the mixture turned from yellow-greenish to yellow-brown, the color of the slides became greenish. The slides were removed from the beaker and rinsed with Milli-Q water. Excess and nonadhesive silver particles on the glass surface were removed by mild sonication of the SIF-coated glass slides for 1 min. As a result of using a sandwiched glass pair for SIF formation, only one side of each slide was coated with SIF. The diameters of the islands are typically 100–500 nm across, and the heights of the islands are ~60 nm. The SIF slides were stored in Milli-Q water until they were used for LbL deposition. SIFs coated on glass slides displayed the characteristic surface plasmon resonance with an absorption maximum near 460 nm.

PSS and PAH at concentrations of 3 and 2 mg/mL, respectively, were dissolved in pure water. All of the polyions are expected to be strongly charged at neutral pH (~6.5). The commercially purchased amine-terminated glass slides were used after drying with air to remove dust particles from the surface. The SIFs were incubated overnight with a 1 mM ethanolic solution of cysteamine and then rinsed with copious amounts of ethanol and Milli-Q water. This step forms a self-assembled monolayer of cysteamine on the surface of the SIFs, and thus SIF surfaces are functionalized with amines and positively charged. Amine-functionalized glass and SIFs were used as substrates. These positively charged substrates were used for polyelectrolyte deposition beginning with a polyanion (PSS in the present case).[25] LbL assembly of PSS/PAH on functionalized glass or SIF substrates was carried out manually. The substrates were immersed in a PSS solution for 20 min, followed by a wash in water for 5 min, and immersed again in the PAH solution for 20 min, followed a wash for 5 min. The water washing between the consecutive adsorptions was effective for successful alternate adsorption. Multilayer assemblies consisting of 1–15 layers of PSS and PAH were prepared by consecutive adsorption of both polyelectrolytes. A schematic representation of the buildup of a multilayer film at the molecular level is shown in Figure 2. A positively charged substrate adsorbs PSS and PAH consecutively; in this example, the counterions have been omitted for clarity. In the outermost layer (PAH in the present case), SRB was adsorbed. It is important to mention that no adsorption of SRB was observed when the outermost layer was PSS. The thickness of the film was varied by inserting different numbers of PSS/PAH layers. We first adsorb SRB directly onto both functionalized glass and SIF surfaces to obtain the probe layer with near 0 nm distance from the surfaces. Subsequently, to get a probe layer with a defined distance from the surfaces, we deposited the required number (i.e., 2, 3, 4, 6, 9, or 15) of PSS/PAH layers (Figure 2). Each layer of the PSS/PAH assembly adds a distance of about 2.1 nm. Subsequently, using 2, 3, 4, 5, 6, 9, and 15 layers of PSS/PAH results in probe layers on SIF surfaces with distances ($d$) of approximately 4.2, 6.3, 8.4, 10.5 12.6, 19, and 32 nm, respectively. After the layers were completely dried at ambient conditions, SRB was incorporated into the PSS/PAH nanocomposite assembly by immersion into an aqueous SRB solution for about 5 min. To avoid any probe aggregation in the LbL assembly, we used the lowest possible concentration of $1 \times 10^{-6}$ M and a short period of immersion time (5 min).[37,38]

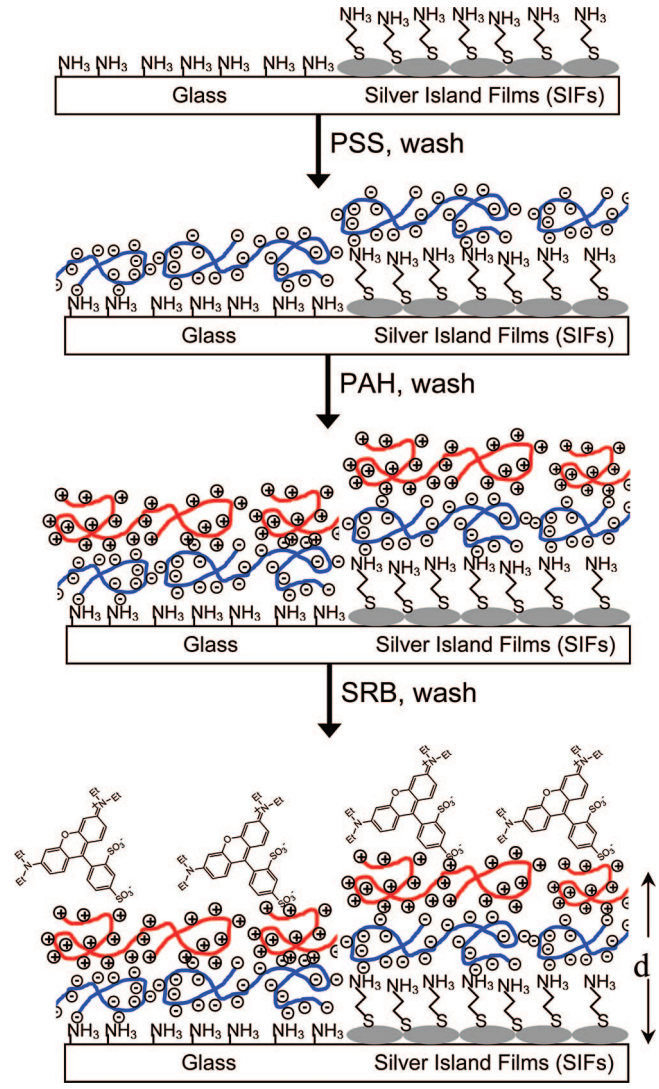


**Figure 2.** Schematic representation of the LbL assembly by adsorption of a polyanion (PSS) and a polycation (PAH). Glass and SIF surfaces were initially functionalized with amines to render a positively charged surface. The thickness of the film was varied by inserting different numbers of PSS/PAH layers. In the final layer, SRB was adsorbed on the PAH layer.

Absorption spectra were taken using a Hewlett-Packard 8453 UV–vis spectrophotometer. Emission spectra of the SRB-incorporated PSS/PAH nanocomposite assembly on both glass and metal nanostructured substrates were recorded by a Varian Cary Eclipse fluorescence spectrophotometer. We have used front-face illumination geometry with 514 nm excitation from a xenon arc lamp. Time-resolved intensity decays were recorded using a PicoQuant Fluotime 100 time-correlated single-photon counting fluorescence lifetime spectrometer. The excitation source was a pulsed laser diode (PicoQuant PDL800-B) with a 20 MHz repetition rate. The instrument response function (IRF) is about 60 ps. Emission lifetimes were measured with vertically polarized excitation. Magic angle observation was used in the emission path for the time-domain measurements. Intensity decays were measured through a bandpass interference filter (Chroma Inc.) in the 570–630 nm spectral region.

(37) Ray, K.; Nakahara, H. *J. Phys. Chem. B* **2002**, *106*, 92.
(38) Ray, K.; Nakahara, H.; Sakamoto, A. *Spectrochim. Acta A* **2005**, *61A*, 103.

Fluorescence intensity decays are usually described as the sum of individual exponentials. The intensity decay following $\delta$-function excitation is described by:[39]

$$I(t) = \sum_{i=1}^{n} \alpha_i e^{-t/\tau_i} \quad (1)$$

where $\tau_i$ are the individual decay times and $\alpha_i$ are the associated preexponential factors. The fractional contribution of the $i$th component to the total emission is written as

$$f_i = \frac{\alpha_i \tau_i}{\sum_j \alpha_j \tau_j} \quad (2)$$

We have normalized the values of $\alpha_i$ and $f_i$ so that $\sum_i \alpha_i = 1.0$ and $\sum_i f_i = 1$. The average lifetime is given by

$$\bar{\tau} = \sum_i f_i \tau_i \quad (3)$$

and the amplitude-weighted lifetime is described as

$$\langle \tau \rangle = \sum_i \alpha_i \tau_i \quad (4)$$

We have extracted the values of $\alpha_i$ and $\tau_i$ using PicoQuant Fluofit 4.1 software (Professional Version) with the deconvolution of IRF and nonlinear least-squares fitting. The goodness-of-fit was judged by the value of reduced $\chi^2$.

We now consider an alternative model to analyze the intensity decay data in which the $\alpha_i$ values are not discrete amplitudes at $\tau_i$ but rather are described by a continuous distribution of $\alpha(\tau)$. The intensity decay then contains components of each lifetime $\tau$ with an amplitude $\alpha(\tau)$. The component with each individual $\tau$ value is given by[39]

$$I(\tau, t) = \alpha(\tau)\, e^{-t/\tau} \quad (5)$$

The total decay law is the sum of the individual decays weighted by the amplitudes

$$I(t) = \int_{\tau=0}^{\infty} \alpha(\tau)\, e^{-t/\tau}\, d\tau \quad (6)$$

where $\int \alpha(\tau)\, d\tau = 1$. Considering a Gaussian distribution, the $\alpha(\tau)$ is given by

$$\alpha_G(\tau) = \frac{1}{\sigma\sqrt{2\pi}} e^{[-(1/2)((\tau - \bar{\tau})/\sigma)^2]} \quad (7)$$

where $\bar{\tau}$ is the central value of the distribution and $\sigma$ is the standard deviation of the Gaussian. For a Gaussian distribution, the full width at half-maximum is given by $2.354\sigma$.[40]

## 3. Results and Discussion

Construction of LbL layers of PSS/PAH on both glass and SIF-coated glass surfaces and subsequent SRB adsorption are performed conveniently as described in the Experimental Details section and shown schematically in Figure 2. The SRB adsorbed in PSS/PAH nanocomposites on a glass surface shows typical absorption and emission band maxima

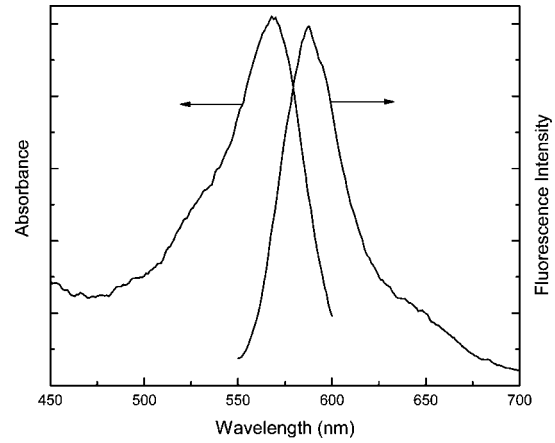


**Figure 3.** Absorption and emission spectra of a SRB-adsorbed PSS/PAH nanocomposite on a glass surface. $\lambda_{ex} = 514$ nm.

at 570 and 587 nm, respectively (Figure 3), resulting presumably from noninteracting monomeric SRB molecules on the surface. This is in accordance with our previous results where we discussed the effect of the SRB concentration and aggregation pattern on both its absorption and emission spectra from a glass surface.[37,38] In the present study, we have particularly chosen the lowest possible dye concentration of $1 \times 10^{-6}$ M and a minimum dye adsorption time to avoid SRB aggregation in the PSS/PAH layer and subsequent complications in the MEF.

The effect of probe orientation on the MEF is not fully explored, and it is not in the scope of this study. However, it is important to determine the orientation of the probe incorporated in the PSS/PAH LbL assembly to help in the understanding of the metal–fluorophore interaction. Polarized visible absorption or IR-attenuated total reflection spectra can provide an indication of the order and orientation of the probes in ultrathin films deposited on solid substrates. In the present case, polarized visible absorption spectra have been used to determine the orientation of the SRB molecule in LbL assembly. Figure 4 shows the absorption spectra measured for a SRB-adsorbed PSS/PAH nanocomposite on glass (only one side of the substrate) at two incident angles. At the normal incidence, the absorption intensities for the p- and s-polarized lights are almost the same. This suggests that the vectors of the transition dipole moments of the SRB molecules are uniformly distributed over the film surface, taking a constant angle with the surface normal. On the other hand, when the film was tilted 45°, the absorption under the s-polarization mode is stronger than that of the p-polarization; the unpolarized absorption falls between the two extremes. A quantitative evaluation of the molecular orientation of the SRB molecule was made by considering four phases, namely, air, LbL assembly, substrate, and air. Assuming a uniaxial orientation of the transition dipole moment with the angle $\theta$, the ratio between p- and s-polarized intensities is[41]

$$\frac{A_p}{A_s} = \frac{n_1 \cos i + n_3 \cos r}{n_2 \cos r + n_3 \cos i} \left\{ \cos i \cos r + \frac{2 n_1^3 n_3 \sin^2 i}{n_2^4 \tan^2 \theta} \right\} \quad (8)$$

where the refractive indices of four phases are assumed to be $n_1 = 1.00$ (air), $n_2 = 1.50$ (LbL film), and $n_3 = 1.54$ (substrate), $i$ is the angle of incidence at the LbL film, and

(39) Lakowicz, J. R. *Principles of Fluorescence Spectroscopy*, 3rd ed.; Springer: New York, 2006.
(40) Bevington, P. R. *Data reduction and error analysis for the physical sciences*; McGraw-Hill: New York, 1969.

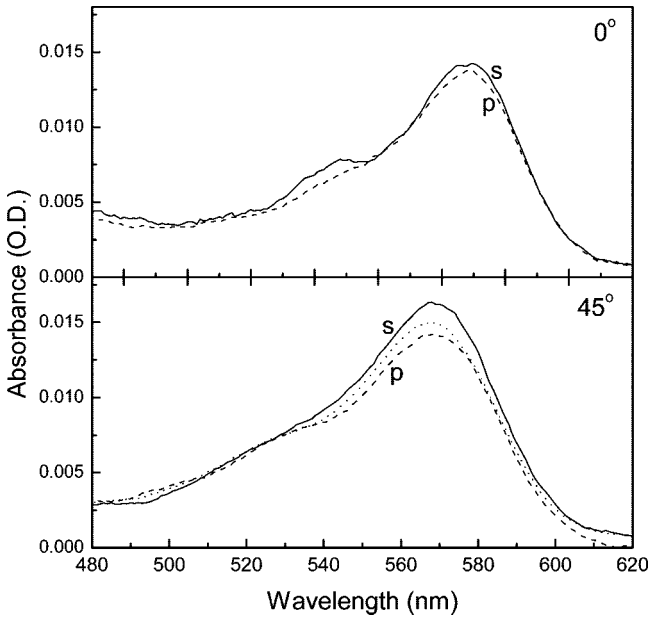


**Figure 4.** Polarized absorption spectra of a SRB-adsorbed PSS/PAH nanocomposite on glass at incidence angles of 0 and 45°. Solid and dashed lines indicate the absorption spectra for s- and p-polarized light, respectively. The observed tilt angle of the SRB transition dipole moment (along the long axis) with respect to the surface normal is ~40°.

$r$ is the angle of refraction at the interface of the LbL film and substrate that can be evaluated from $n_1 \sin i = n_3 \sin r$. $\theta$ is the tilt angle of the transition dipole moment of the SRB probe molecule with respect to the surface normal. From the above equation, we evaluated the tilt angle, $\theta$, of 40° for the SRB molecule adsorbed with the PAH layer. Because the direction of the transition moment of the SRB molecule is assigned along the long axis, this measurement suggests that the SRB molecule tilted considerably from the surface normal, as shown schematically in Figure 2. Additionally, it is worthwhile to mention that we observed very similar probe orientation irrespective of the probe distance from the glass surface.

Subsequently, after exploring the photophysical properties and orientation of the adsorbed SRB probe molecule on the PSS/PAH assembly, we performed a detailed investigation on the SRB-adsorbed PSS/PAH nanocomposites on the metal-nanostructured surfaces. The fluorescence emission spectrum of SRB incorporated into PSS/PAH layers with a ~8.4 nm probe separation distance from SIF surfaces is shown in Figure 5 (top panel). The corresponding emission spectrum of SRB on PSS/PAH nanocomposites on a glass surface is also included in the plot for comparison. To obtain a meaningful comparison, we maintained all of the experimental settings while collecting the fluorescence emission spectra from both substrates. The SRB absorbed in the PSS/PAH LbL assembly has an emission band maximum of ~587 nm from both glass and SIF surfaces. Interestingly, we have observed very similar spectral features, except differences in their intensities, from the probe on both glass and SIF surfaces. The intensity-normalized emission spectra of a SRB-adsorbed LbL assembly on both glass and SIF surfaces

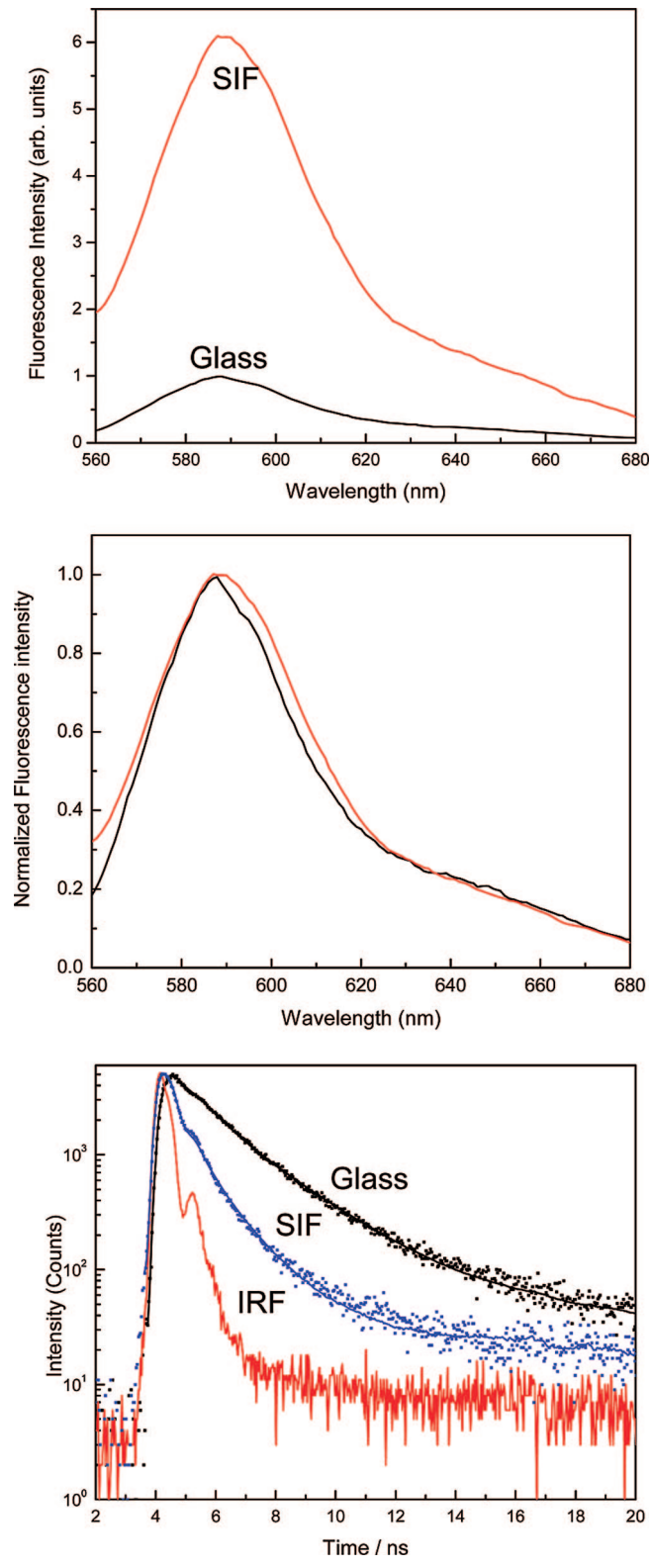


**Figure 5.** Fluorescence emission spectra of a SRB-adsorbed PSS/PAH assembly on SIF and glass surfaces (top panel), corresponding intensity-normalized spectra (middle panel), and SRB intensity decays from metalized and nonmetalized areas (bottom panel). The IRF also included in the figure.

are shown in Figure 5 (middle panel).

We recorded the time-domain intensity decays from the SRB-adsorbed PSS/PAH layers on both glass and SIF surfaces. Intensity decays observed for the SRB on glass and SIFs with a probe distance of ~8.4 nm from the surfaces

(41) Stanescu, M.; Samha, H.; Peristein, J.; Whitten, D. G. *Langmuir* **2000**, *16*, 275.

are depicted in Figure 5 (bottom panel). The solid lines indicate the best fit to the experimental decay curves. As can be seen from the figure, SRB shows faster intensity decay on the SIF surface as compared to that on the glass surface. Accordingly, we observed a ~3-fold shortening in the lifetime from the SIF surface. This shortening of the lifetime and the observed increase in the fluorescence intensity on the SIF surface (Figure 5) are presumably due to the interaction of SRB molecules with the silver nanoparticles. We have taken sufficient precautions to make sure the observed reduced lifetime, especially the short component in the probe intensity decay from the SIF surface is not due to the scattered light but to the SRB emission. This is because noble metal colloids show strong scattering properties, and the scattering from colloids may contribute to the observed short lifetime. To determine contributions from SIF scattering on the observed lifetimes, we performed a set of control experiments on the glass and SIF substrates without any dye molecule on the PSS/PAH layers. We observed almost no signal with the combination of filters used to detect the SRB emission, indicating that the observed reduction in lifetimes is the result of near-field interactions of SRB with SIF surfaces. The increase in the emission intensity and the decrease in the fluorescence lifetime suggest an increased radiative decay rate in the presence of metal nanoparticles and are in accordance with the radiative decay engineering model.[9,10]

To study the distance effect on the MEF, we conducted a systematic sets of experiments on SRB-adsorbed PSS/PAH nanocomposites assembled on both glass and SIF surfaces, where the SRB distance is varied from 0 to 32 nm from the surfaces. Figure 6 (top panel) shows the fluorescence emission spectra from SRB-adsorbed PSS/PAH layers with varied probe distances from the SIF surface. The fluorescence spectra and emission intensities from the SRB-adsorbed PSS/PAH nanocomposite at different distances from the glass surfaces are similar. On the other hand, SRB from the SIF surface shows significant changes in the fluorescence intensities with the distances between the metal and the fluorophore. The enhancement factors (the ratios between the integrated areas under the spectral region) of SRB on SIFs over glass surfaces are plotted as a function of the metal–fluorophore distance (shown in Figure 6, bottom panel). The largest enhancement of ~6-fold is observed for the SRB-adsorbed PSS/PAH nanocomposite with the probe distance of 8.4 nm from the SIF surface. The intensity relative to the glass surfaces decreases progressively with an increase in the number of PSS/PAH layers to an enhancement near 1.5-fold for 15 layers of the PSS/PAH assembly. Interestingly, we have also observed a monotonic reduction in the fluorescence intensity (from 6-fold to 0.5-fold) with a decrease in the probe distance from 8.4 to 0 nm. The present study shows that the MEF is distance-dependent. The decrease in the fluorescence enhancement below a 8.4 nm distance from the metalized surfaces could be related to the usual quenching of emission when the fluorophores are in close proximity to the metals.

Time-resolved fluorescence measurements provide a wealth of information related to the system under investigation and

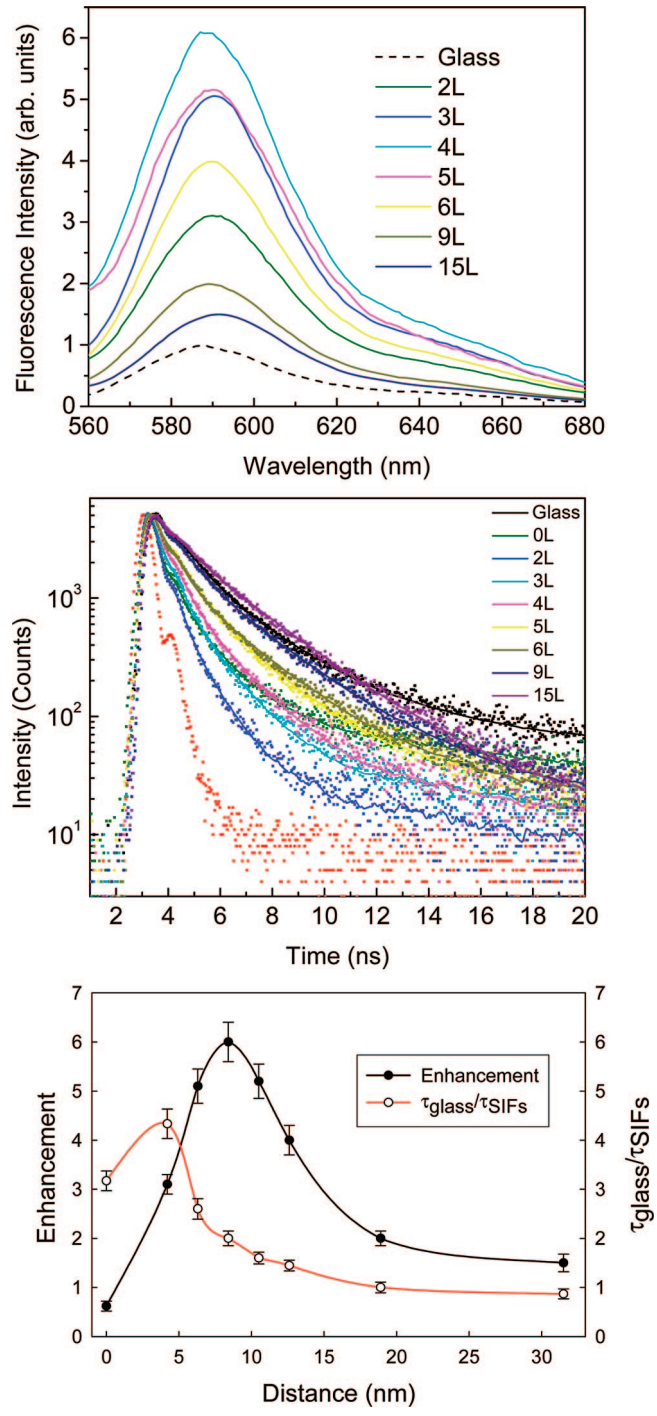


**Figure 6.** Effect of SRB to SIF surface distances on the fluorescence intensity (top panel) and the fluorescence lifetime (middle panel). The bottom panel shows the effect of the probe distance on the fluorescence enhancement and the ratios of average lifetime $\tau_{glass}/\tau_{SiFs}$.

the microenvironments around the fluorophores.[39] A combination of quantum yields with the lifetimes of SRB incorporated on PSS/PAH nanocomposites on glass and SIF surfaces will provide more insights into its distance-dependent metal–fluorophore interactions. Subsequently, we measured the fluorescence intensity decays for all SRB-adsorbed PSS/PAH nanocomposites assembled on both SIF and glass surfaces. Figure 6 (middle panel) shows the corresponding fluorescence intensity decays from the SIF surface. SRB-adsorbed PSS/PAH nanocomposites on SIFs with varied distances show significant changes in the intensity decays,

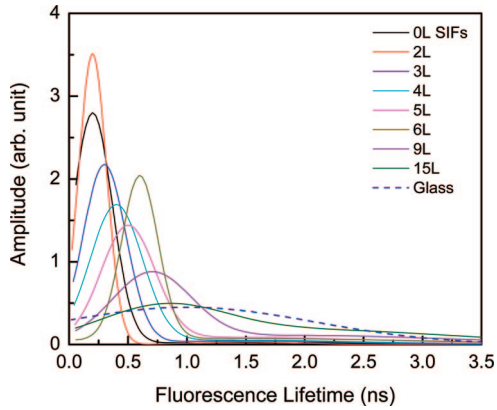


**Figure 7.** Fluorescence lifetime distributions of the SRB monolayer at multiple distances from the SIF surface. A lifetime distribution of the SRB monolayer on a glass substrate is also included for comparison.

whereas the corresponding intensity decays from glass are insensitive to the probe distance from the surface (not shown). The intensity decay of a SRB-adsorbed PSS/PAH assembly on glass is also included in Figure 6 (middle panel). The shortest intensity decay was observed at a distance of 4.2 nm from the metal. The average lifetimes are consistently increased with an increase in the distance from the SIF surface from 4.2 to 32 nm. Furthermore, the SRB layer within the contacting distance (i.e., 0 nm) from the SIF surface shows longer decay than the SRB probes positioned at a distance of 4.2 nm from the SIF surface. One explanation of this effect is that the SRB molecules directly on the silver surface are quenched, and the observed decay is due to SRB molecules in the region of the slide, which are distant from the metal. The ratio of the average lifetimes of each particular probe layer on glass and that on the SIF surface was plotted as a function of the distance from the SIF surface (Figure 6, bottom panel). The highest factor of reduction in the fluorescence lifetime of about 4.5-fold is observed from the SRB-adsorbed PSS/PAH nanocomposite layer with 4.2 nm distance from the SIF surface. When the fluorophores are spaced by 32 nm distance from the metal surface, the emission lifetimes of SRB-adsorbed PSS/PAH nanocomposite layers on SIF and glass surfaces are nearly the same. The reduction in the fluorescence lifetime on the SIF surfaces at distances from 0 to 20 nm could result from an increase in the radiative decay rate as well as could be due to increased nonradiative interactions between the metal and fluorophore.

These metal-nanostructured substrates are inherently heterogeneous. To unravel the heterogeneity in the distribution of fluorophores on metal-nanostructured substrates, we have analyzed the intensity decay kinetics using an alternative model, which allows for a continuous distribution of decay times. We have performed a comparative study on the lifetime distributions of the probe incorporated in the PSS/PAH nanocomposite assembly on glass and SIF surfaces (Figure 7). We have observed similar distributions of SRB molecules for different distances from the glass substrate (not shown). A representative lifetime distribution of the SRB incorporated in the LbL assembly on glass surfaces is shown in Figure 7. The major lifetime distribution that centers around 250 ps is observed when the SRB molecules are directly on the SIF surface. The measured lifetime distributions of the SRB probe, as presented in Figure 7, show an interesting trend when assembled on the SIF surface and are generally the center of the short (major) lifetime distribution shifts toward longer lifetimes with an increase in the distance between metal and fluorophores. The full width at half-maxima (fwhm) of the Gaussian distributions on SiF surfaces are systematically increased as a function of the increasing distance between the metal and fluorophores. The center of the lifetime distribution is indicative of the average microenvironments surrounding the SRB probe, while the distribution width is related to the range of environments.[42]

The present study clearly shows that the fluorescence intensities, or, in other words, the quantum efficiencies, and radiative decay rates vary as a function of the metal–fluorophore distance. In general, the quantum yield and lifetime of a fluorophore are described as[9,10]

$$\Phi_0 = \frac{\Gamma}{\Gamma + k_{nr}} \tag{9}$$

$$\tau_0 = \frac{1}{\Gamma + k_{nr}} \tag{10}$$

where $\Gamma$ and $k_{nr}$ are the radiative and nonradiative decay rates, respectively. In proximity to the metallic surfaces and/or particles, eqs 9 and 10 are modified as

$$\Phi_m = \frac{N_r\Gamma}{N_r\Gamma + k_{nr}'} \tag{11}$$

$$\tau_m = \frac{1}{N_r\Gamma + k_{nr}'} \tag{12}$$

The radiative decay rate is increased to $N_r\Gamma$ in the presence of plasmonic metal nanostructures. $k_{nr}'$ is the nonradiative decay rate in the presence of metal particles. The ratio of fluorescence quantum yields in the presence and absence of metal is interrelated as

$$\frac{\Phi_m}{\Phi_0} = \frac{N_r(\Gamma + k_{nr})}{N_r\Gamma + k_{nr}'} = \frac{N_r\tau_m}{\tau_0} \tag{13}$$

The changes in the rates of emission ($N_r$) and excitation ($N_{ex}$) as a function of the metal–fluorophore distance ($d$) could be written as

$$N_r(d) = N_r^{d=0}\exp\left(-\frac{d}{R_r}\right) + 1 \tag{14}$$

$$N_{ex}(d) = N_r^{d=0}\exp\left(-\frac{d}{R_{ex}}\right) + 1 \tag{15}$$

$R_r$ and $R_{ex}$ are the characteristic distances over which $N_r$ and $N_{ex}$ decrease to 1/e exponentially. The measured emission intensity with ($I_m$) or without ($I_0$) metal could be related as

$$I_m = I_0\frac{\Phi_m}{\Phi_0}N_{ex}(d) \tag{16}$$

Combining eqs 13–16, the total fluorescence intensity could more explicitly be written as

(42) D'Auria, S.; Bazzicalupo, P.; Rossi, M.; Gryczynski, I.; Lakowicz, J. R. *J. Fluoresc.* **2000**, *10*, 27.

$$I_m = I_0 \frac{\tau_m}{\tau_0}\left[N_r^{d=0} \exp\left(-\frac{d}{R_r}\right) + 1\right]\left[N_{ex}^{d=0} \exp\left(-\frac{d}{R_{ex}}\right) + 1\right] \quad (17)$$

We analyzed our experimental steady-state intensities and fluorescence lifetimes data of SRB at various distances from the plasmonic metal-nanostructured surfaces. By fitting the experimental steady-state and time-resolved data with eq 17, the values of the free parameters $N_r^{d=0} = 5$, $N_{ex}^{d=0} = 10$, $R_r = 17$ nm, and $R_{ex} = 5$ nm were obtained. Furthermore, our analysis reveals that the rate of excitation is increased by a factor of 10 and arises at a distance of 5 nm, whereas the increase in the radiative decay rate is 5-fold and this increase continues over a distance of ~17 nm. The radiative decay and excitation rates were extracted from the spectral parameters and are plotted as a function of metal–fluorophore distance, as shown in Figure 8. It is apparent from the normalized distance-dependent plot that the increases in radiative decay occur up to a distance of ~20 nm and the enhanced excitation takes place below ~10 nm.

## 4. Summary

In this study, we have controlled the metal–fluorophore distance by a polyelectrolyte alternate LbL assembly technique. We examined the steady-state and time-resolved fluorescence spectral property of SRB at various distances from the metal-nanostructured surfaces. SRB-adsorbed LbL assembly of anionic and cationic polyelectrolytes PSS and PAH was successfully utilized to explore the distance-dependent nature of MEF. Our results summarize that maximum fluorescence enhancements occur about 8–9 nm from the metal-nanostructured surface, a distance that could readily be obtained by one or two layers of proteins. Lifetime distributions have been recovered from fluorescence decay curves to unravel the heterogeneity in the distribution of SRB probes in the nanocomposite assembly. The bimodal distribution appears to be an acceptable description of the lifetime of the SRB adsorbed on the PSS/PAH LbL assembly at varied distances from the plasmonic nanostructured surfaces. This lifetime distribution analysis is a useful tool in the surface photophysical studies especially when the fluorophores are located in proximity to the heterogeneous plasmonic nanostructured surfaces.

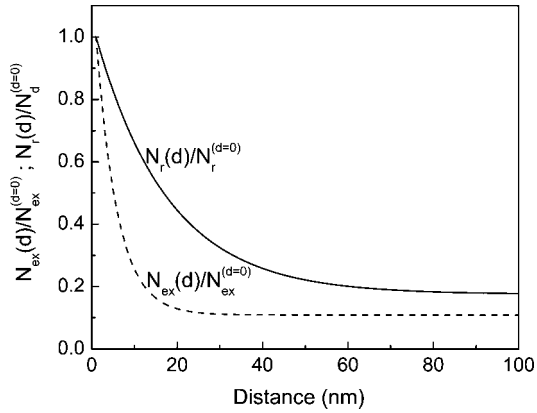


**Figure 8.** Normalized rate of excitation [$N_{ex}(d)/N_{ex}^{d=0}$] and rate of radiative decay [$N_r(d)/N_r^{d=0}$] as a function of the distance from the metal surface.

**Acknowledgment.** This research was supported by the National Center for Research Resources (Grant RR-08119) and the National Institute of Biomedical Imaging and Bioengineering (Grants EB-00682 and EB-0065211) and the National Human Genome Research Institute (Grant HG-002655).

CM071510W